

Interacting exciton-polaritons in cylindrical micropillars

Yury S. Krivosenko,¹ Ivan V. Iorsh,¹ and Ivan A. Shelykh^{1, a)}

Department of Physics and Engineering, ITMO University, St. Petersburg 197101, Russia

(*Electronic mail: y.krivosenko@gmail.com)

We present a quantitative microscopic analysis of the formation of exciton-polaritons, the composite particles possessing light and material components, polariton-polariton interactions, and resonant pumping dynamics in cylindrical semiconductor micropillars. We discuss how the redistribution effect can be used in devices generating photons with non zero orbital angular momenta.

I. INTRODUCTION

Cavity polaritons, also known as exciton-polaritons^{1–3} are composite quasiparticles consisting of excitonic and a photonic components. Conventional geometry where polaritons can be routinely observed is a planar semiconductor microcavity, which consists of a semiconductor quantum well, sandwiched between a pair of distributed Bragg reflectors (DBRs) and placed in the position where photonic mode of such Fabry-Perot cavity has an antinode.

The physics of polaritons attracted substantial interest of the researches working in the domains of photonics and condensed matter physics. This is mainly due to the unique properties of polaritons, related to their composite nature. The combination of extremely low effective mass, inherited from the photonic component, with giant nonlinear optical response, stemming from the excitonic part, enables the observation of a set of intriguing collective phenomena at surprisingly high temperatures^{2,4,5}. Examples include polariton BEC and polariton lasing^{6–9}, formation of topological defects such as solitons^{10–13}, quantized vortices^{14,15} and vortex lattices^{16,17}, skyrmions and merons^{18,19}, shock waves²⁰ and many others. Moreover, polariton systems can form a basis for creation of nanophotonic devices of the next generation, including optical logic gates and all-optical integrated circuits^{21–24}.

The visible current trend in polaritonics is the shift towards quantum applications^{25–27}. Geometries with cavity polaritons were suggested as candidates for creation of the sources of single photons^{28–32} and entangled photon pairs^{33–35}, the corresponding onset of polaritonic quantum correlations was reported^{36–39}. Moreover, the possibility to use polariton systems in quantum computing^{40,41} and as quantum and neuro-morphic simulators was actively discussed^{41–46}.

For applications of polaritonics at the quantum level two ingredients are necessary: spatial confinement of the polaritons and pronounced nonlinearity. The first can be achieved by etching of a planar microcavity, which allows to get individual polariton pillars^{47–52}, systems of several coupled pillars forming so-called polariton molecules⁵³ or periodically arranged arrays of the pillars forming polariton superlattices^{43,54–56}. As for polariton nonlinearity, it is provided by the excitonic fraction, and the main contribution is given by the exchange

interaction of electrons and holes forming the excitons^{57–61}. The quantitative analysis of the polariton nonlinearities in micropillars is thus an important problem, which we solve in the current work.

We consider in detail the formation of exciton-polaritons in cylindrical micropillars, develop a microscopic theory for the calculation of the matrix elements of polariton-polariton interaction in this geometry, and analyze nonlinear dynamics of such a system subject to a partially coherent pumping, investigating, in particular, the redistribution of energy between polaritonic states with different angular momenta.

The paper is organised as follows. In sections II A, II B, and II C we briefly describe the formation of the photonic cavity modes, quantum-well excitonic modes (accounting for exciton-exciton interaction), and polaritonic modes, respectively. In section II D we consider the dynamics of the coherently pumped polaritons. Section III contains numeric results and their discussion. Conclusions are summarized in section IV. Appendices contain the technical details of the calculations.

II. THEORY

The system we consider is schematically shown in Figure 1 (left panel). It consists of a semiconductor micropillar with cylindrical symmetry (grey cylinder) flanked by a pair of dielectric Bragg mirrors (DBRs, the orange planes), and containing a quantum well (QW, the green circle in the middle) placed in the position of an antinode of an electric field of the optical cavity mode. The energy of the cavity mode is brought close to the resonance to the energy of the excitonic transition, favoring the formation of the hybrid polariton modes.

As polaritons contain an excitonic fraction, they interact with each other. The scheme of the polariton-polariton interaction is shown in the right panel of Figure 1. As the system we consider has cylindrical symmetry, polaritons are characterized by their projections of angular momenta (λ_j) onto the structure growth axis. States with different angular momenta have different profiles of their wave functions, shown schematically by the purple surfaces. Polaritons can exchange their angular momenta due to the exciton-exciton scattering, which, obviously, conserve the total angular momentum.

The Hamiltonian of the interacting excitons coupled to a photonic cavity mode is:

$$\hat{H}_{\text{tot}} = \hat{H}_x + \hat{H}_p + \hat{H}_{xp} + \hat{H}_{xx}, \quad (1)$$

^{a)}Science Institute, University of Iceland, Dunhagi 3, IS-107, Reykjavik, Iceland

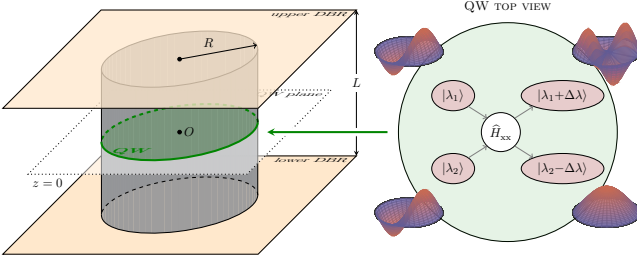


FIG. 1. Left panel: Sketch of the considered geometry, consisting of a semiconductor micropillar (grey cylinder) flanked by a pair of dielectric Bragg mirrors (DBRs, the orange planes), and containing a quantum well (QW, the green circle in the middle) placed in the position of an antinode of an electric field of the optical cavity mode. The energy of the cavity mode is brought close to the resonance to the energy of the excitonic transition, giving rise to the formation of the polaritons. Right panel: Top view of the system illustrating the scheme of the exciton-exciton scattering. Excitons in the states $|\lambda_1\rangle$, $|\lambda_2\rangle$, $|\lambda_1+\Delta\lambda\rangle$, and $|\lambda_2-\Delta\lambda\rangle$ (the red rounds) are coupled via interaction Hamiltonian \hat{H}_{xx} (the white round). Excitonic wave functions $\lambda_1=\lambda_2=\Delta\lambda=1$ and $v_{1,2,3,4}=1$ are schematically shown by purple surfaces next to the states markers.

where, \hat{H}_x and \hat{H}_p are Hamiltonians of free excitons and photons, \hat{H}_{xp} and \hat{H}_{xx} are Hamiltonians of photon-exciton and exciton-exciton interaction, respectively.

In second quantization representation, they can be written as:

$$\hat{H}_x = \sum_{\lambda, \nu} \hbar\Omega_{\lambda\nu} \hat{X}_{\lambda\nu}^\dagger \hat{X}_{\lambda\nu} = \sum_{\kappa} \hbar\Omega_{\kappa} \hat{X}_{\kappa}^\dagger \hat{X}_{\kappa}, \quad (2a)$$

$$\hat{H}_p = \sum_{l, n} \hbar\omega_{ln} \hat{a}_{ln}^\dagger \hat{a}_{ln} = \sum_k \hbar\omega_k \hat{a}_k^\dagger \hat{a}_k, \quad (2b)$$

$$\hat{H}_{xp} = \sum_{k, \kappa} \hbar \left(g_{k\kappa} \hat{X}_{\kappa}^\dagger \hat{a}_k + \text{h.c.} \right), \quad (2c)$$

$$\hat{H}_{xx} = \frac{1}{2} \sum_{\kappa_1 \kappa_2 \kappa_3 \kappa_4} V_{\kappa_1 \kappa_2 \kappa_3 \kappa_4} \hat{X}_{\kappa_1}^\dagger \hat{X}_{\kappa_2}^\dagger \hat{X}_{\kappa_3} \hat{X}_{\kappa_4}. \quad (2d)$$

Here, $\hat{X}_{\lambda\nu}^{(\dagger)}$ and $\hat{a}_{ln}^{(\dagger)}$ are the $\lambda\nu$ -excitonic and ln -photonic mode annihilation (creation) operators, respectively, and $\hbar\Omega_{\lambda\nu}$ and $\hbar\omega_{ln}$ are the corresponding eigenenergies. The indices λ and ν (l and n) are the excitonic (photonic) angular and radial quantum numbers, respectively. In equation (2c), $\hbar g_{k\kappa} \equiv \hbar g_{ln\lambda\nu}$ represent the amplitudes of the interaction between $\lambda\nu$ -excitonic and ln -photonic modes. To spare the notations, we hereafter denote the pairs of the excitonic, $\lambda_{(j)}\nu_{(j)}$, and photonic, $l_{(j)}n_{(j)}$, indices as $\kappa_{(j)}$ and $k_{(j)}$, respectively.

A. Photonic modes

To analyze the photonic modes in the cylindric symmetry microcavity, we follow the scheme of the reference 62. We consider a microcavity placed between a pair of DBRs and containing a cylindric micropillar of a radius R made of a semiconductor with high-frequency dielectric permittivity ϵ_1 .

The effective inter-DBRs distance is denoted as L . Within the conventional cylindric coordinates frame (r , z , and θ), the z -component of the field is sought as a product of Bessel's functions (BFs) of either the first kind (core region, argument $\beta_1 r$) or the modified BF (air region, argument $\beta_2 r$), the complex exponential of $(i l \theta)$, and $\cos \alpha z$. This introduces the radial, angular, and z dependences, respectively. The value α is chosen to be π/L which corresponds to the fundamental (in z -direction) photonic mode and obeys the zero boundary conditions at the cylinder bases ($z = \pm L/2$).

The use of the continuity condition for the fields tangential components at the core-to-vacuum boundary ($r = R$) leads to the characteristic equation (see (A2)) and the photonic target function (PTF):

$$\mathcal{F}_{\text{ptf}}(\hbar\omega) = u^4 v^4 (\eta_1 + \eta_2) (k_1^2 \eta_1 + k_2^2 \eta_2) - l^2 \alpha^2 (u^2 + v^2)^2, \quad (3a)$$

where

$$\eta_1 = \frac{J_l'(u)}{u J_l(u)}, \quad \eta_2 = \frac{K_l'(v)}{v K_l(v)}, \quad u = \beta_1 R, \quad v = \beta_2 R. \quad (3b)$$

The PTFs are displayed in Fig. 2 as vertically oriented curves. Their roots (photonic modes eigenenergies) are marked by the round grey symbols.

The core-region (index 1), air-region (index 2) quasimomenta $\beta_{1,2}$, and frequency ω are interconnected by

$$\beta_1^2 = \frac{\omega^2 \epsilon_1}{c^2} - \alpha^2, \quad \beta_2^2 = \alpha^2 - \frac{\omega^2 \epsilon_2}{c^2}. \quad (3c)$$

The system of eqs. (3) is invariant under the $l \rightarrow -l$ substitution and, hence, is solved only for $l \geq 0$. The procedure results in a set of frequencies numbered by the index n for each l : ω_{ln} , $n = 1, 2, \dots, N(|l|)$.

All the details of the computational procedure are presented in Appendix A.

B. Excitonic modes

Considering the excitonic part, we use the following assumptions:

$$R \gg a_{\text{Bohr}} \gg a_{\text{u.c.}}, \quad (4)$$

where a_{Bohr} is the two-dimensional exciton Bohr radius, and $a_{\text{u.c.}}$ is the characteristic size of the micropillar material unit cell. These conditions allows to neglect the internal structure of excitons when considering their confinement inside a pillar. Moreover, the excitonic density n_X is supposed to be small enough to treat them as bosons, i.e. the following condition is satisfied:

$$n_X a_{\text{Bohr}}^2 \ll 1. \quad (5)$$

The dielectric-to-vacuum boundary is assumed to be an infinite barrier.

Inside the cavity, we can factorize the excitonic wave function as

$$\phi_{\kappa}(\mathbf{r}, \rho) = \Phi_{\lambda\nu}(\mathbf{r}) \chi_{1s}(\rho), \quad (6)$$

where $\Phi_{\lambda\nu}(\mathbf{r})$ describes the exciton centre-of-mass motion, and $\chi_{1s}(\rho)$ corresponds to the relative motion of an electron and a hole, and for conventional semiconductor materials can be well approximated by the two-dimensional hydrogen-like atom wave function (in this paper, we consider only the 1s excitonic ground state):

$$\Phi_{\lambda\nu}(\mathbf{r}) = \frac{J_{\lambda}(\alpha_{\lambda\nu} r) \exp i\lambda\theta}{|J_{|\lambda|+1}(\alpha_{\lambda\nu})| R\sqrt{\pi}}, \quad (7a)$$

$$\chi_{1s}(\rho) = \frac{\exp(-\rho/a_{\text{Bohr}})}{a_{\text{Bohr}}} \sqrt{\frac{2}{\pi}}. \quad (7b)$$

The quantum numbers λ and ν are thus associated with the exciton centre-of-mass motion, $x_{\lambda\nu}$ is the ν th root of BF J_{λ} , and $\alpha_{\lambda\nu} = x_{\lambda\nu}/R$.

The excitonic energies are expressed as:

$$\hbar\Omega_{\lambda\nu} = \frac{\hbar^2}{2(m_e^* + m_h^*)} \left(\frac{x_{\lambda\nu}}{R}\right)^2 - \frac{2\hbar^2}{\mu a_{\text{Bohr}}^2} + E_g \quad (8)$$

with m_e^* and m_h^* being the electron and hole effective masses, respectively, μ – the effective reduced mass of an electron-hole pair, and E_g – the semiconductor energy band gap. The second term in (8) is the 1s-state eigenenergy.

For realistic cavity parameters, we got that the first term, responsible for the dimensional quantization energy of the motion of the center of the mass is orders of magnitude smaller, then last two terms, so we can neglect the excitonic dispersion and take the energies of all excitonic states to be the same,

$$\hbar\Omega_{\lambda\nu} = \hbar\Omega_x = \text{const}, \quad (9)$$

which is in agreement with the reference 63.

The matrix element of the exciton-exciton scattering $|\kappa_3, \kappa_4\rangle \rightarrow |\kappa_1, \kappa_2\rangle$ in the Born approximation can be written as

$$V_{\kappa_1 \kappa_2 \kappa_3 \kappa_4} = \langle \kappa_1, \kappa_2 | V_{\text{int,xx}} | \kappa_3, \kappa_4 \rangle, \quad (10a)$$

where $|\kappa_i, \kappa_j\rangle$ is the two-exciton wave function antisymmetric with respect the electron-electron and hole-hole exchange:

$$|\kappa_i, \kappa_j\rangle = \frac{1}{2} \cdot \left[\phi_{\kappa_i}(e1, h1) \phi_{\kappa_j}(e2, h2) + \phi_{\kappa_i}(e2, h2) \phi_{\kappa_j}(e1, h1) - \phi_{\kappa_i}(e1, h2) \phi_{\kappa_j}(e2, h1) - \phi_{\kappa_i}(e2, h1) \phi_{\kappa_j}(e1, h2) \right] \quad (10b)$$

with e1(2) and h1(2) presenting the electron and hole coordinates, respectively.

Within the same notations, the matrix elements of the exciton-exciton interaction potential, $V_{\text{int,xx}}$, can be presented as⁶⁴

$$V_{\text{int,xx}} = V_C(e1, h2) - V_C(e1, e2) + V_C(e2, h1) - V_C(h1, h2). \quad (10c)$$

Here, $V_C(\mathbf{r}_1, \mathbf{r}_2) = -e^2/4\pi\epsilon_0\epsilon_{\text{st}}|\mathbf{r}_1 - \mathbf{r}_2|$ is Coulomb potential, ϵ_{st} is the micropillar static dielectric permittivity, e is the elementary charge. The matrix element (10a) can be expressed as the sum $V_{\kappa_1 \kappa_2 \kappa_3 \kappa_4}^{\text{dir}} + V_{\kappa_1 \kappa_2 \kappa_3 \kappa_4}^{\text{xx}} + V_{\kappa_1 \kappa_2 \kappa_3 \kappa_4}^{\text{ee}} + V_{\kappa_1 \kappa_2 \kappa_3 \kappa_4}^{\text{hh}}$ that reveals the four channels (direct, excitons exchange, electron-electron, and hole-hole exchange ones, respectively).

The two latter terms jointly form the fermion-fermion exchange channel, $V_{\kappa_1 \kappa_2 \kappa_3 \kappa_4}^{\text{fx}}$, which gives the major contribution⁶⁴ and is only retained in our further consideration. The corresponding interaction matrix element is

$$V_{\kappa_1 \kappa_2 \kappa_3 \kappa_4} = - \int \dots \int d^8\tau \phi_{\kappa_1}^*(e1, h1) \phi_{\kappa_2}^*(e2, h2) V_{\text{int,xx}} \times \left[\phi_{\kappa_3}(e1, h2) \phi_{\kappa_4}(e2, h1) + \phi_{\kappa_3}(e2, h1) \phi_{\kappa_4}(e1, h2) \right], \quad (10d)$$

where $d^8\tau$ denotes the coordinate phase space volume differential. The elements $V_{\kappa_1 \kappa_2 \kappa_3 \kappa_4}^{\text{dir,xx,fx}}$ respect the angular momentum conservation law, i.e. $V_{\kappa_1 \kappa_2 \kappa_3 \kappa_4}^{\text{dir,xx,fx}} = 0$ if $\lambda_1 + \lambda_2 \neq \lambda_3 + \lambda_4$, which can be schematically written down in terms of the transferred angular momentum $\Delta\lambda$ in the scattering channel:

$$|\lambda_1\rangle + |\lambda_2\rangle \leftrightarrow |\lambda_1 + \Delta\lambda\rangle + |\lambda_2 - \Delta\lambda\rangle. \quad (11)$$

C. The Hamiltonian in the polariton basis

Within the dipole approximation, the operator of exciton-photon interaction can be put down as

$$V_{\text{int,ln}} = -(\mathbf{d}_{\text{cv}} \cdot \mathbf{E}_{ln}), \quad (12)$$

where ln denotes the photonic mode, \mathbf{d}_{cv} is the dipolar matrix element between valence and conduction bands. For the case of GaAs material (studied here), \mathbf{d}_{cv} can be expressed as⁶⁵

$$\mathbf{d}_{\text{cv}} = \frac{d_{\text{cv}}}{\sqrt{2}}(e_x + ie_y) = \frac{d_{\text{cv}}}{\sqrt{2}}(e_r + ie_\theta)e^{i\theta} = \mathbf{d}_{\text{cv}}^0 e^{i\theta}. \quad (13)$$

Then, the exciton-photon interaction matrix element can be presented as the excitonic radiative linewidth multiplied by the overlap of the excitonic and photonic modes wave functions. Following the deduction of reference 63, we eliminate the extra phase factor $e^{i\theta}$ in (13) and arrive at the following expression for the interaction term:

$$\hbar g_{ln\lambda\nu} = -\chi_{1s}^*(0) \iint_{\text{QW}} \Phi_{\lambda\nu}^*(\mathbf{r}) [\mathbf{d}_{\text{cv}}^0(\mathbf{r}) \cdot \mathbf{E}_{ln}(\mathbf{r})]_{z=0} d^2\mathbf{r} \quad (14)$$

Utilizing the expression for the planar 2D microcavity Rabi splitting ($\hbar\Omega_{2D}$, see Appendix B), we recast the matrix element as

$$\hbar g_{ln\lambda\nu} = -\frac{\hbar\Omega_{2D}}{2} \sqrt{\frac{\epsilon_0\epsilon_1 L}{2\hbar\Omega_x}} \iint_{\text{QW}} \Phi_{\lambda\nu}^*(\mathbf{r}) E_{ln,\parallel}(\mathbf{r}) d^2\mathbf{r}, \quad (15)$$

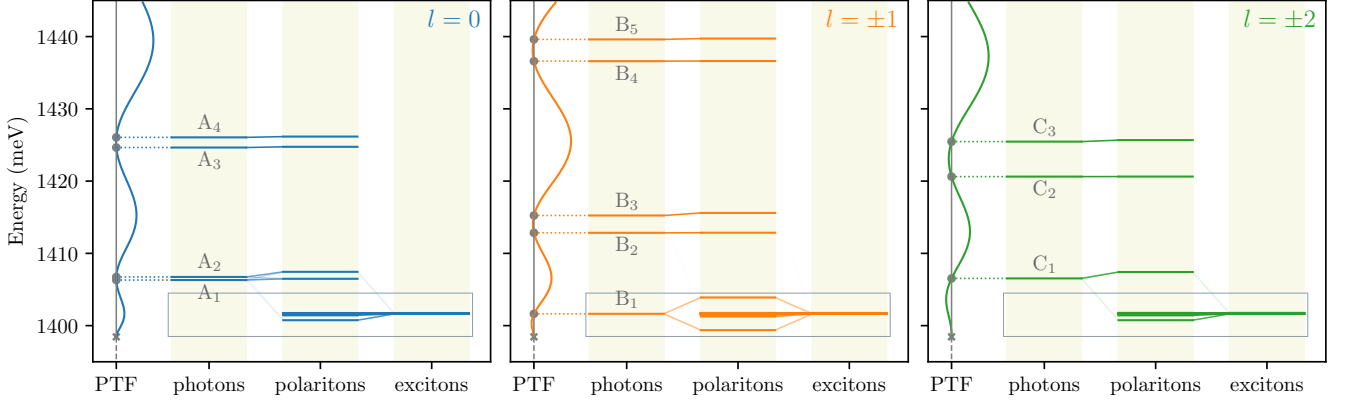


FIG. 2. The photonic target functions (3a) and hybridization schemes of exciton-polaritons formation for $l = 0, \pm 1, \pm 2$ angular quantum numbers. The vertical line at each PTF part shows the zero-PTF axis, the grey rounds and x-markers – the PTFs roots and lower photonic cut-off energies, respectively, the horizontal lines – the energy levels of photons (left), excitons (right), and polaritons (mid). The slant connection lines transparencies indicate the corresponding Hopfield coefficients (HCs) absolute values (the lower the value of the HC, the more the transparency). The open grey rectangles highlight the areas shown in Fig. 3. The micropillar is made of GaAs and has the radius $R = 1.5 \mu\text{m}$, its effective height (134.5 nm). The 2D Rabi splitting is 3.2 meV.

where $E_{ln,||}(\mathbf{r}) = [E_{ln,r}(\mathbf{r}) + iE_{ln,\theta}(\mathbf{r})]_{z=0}$ is the sum of the in-plane radial and angular projections of the cavity mode electric field (with the latter projection being multiplied by imaginary unit). Note, that due to the rotational symmetry only the excitons and photons possessing the same angular momentum ($l=\lambda$) are coupled, so that $\hbar g_{ln\lambda\nu} = 0$ for $l \neq \lambda$. The corresponding explicit expressions are presented in Appendix B.

The linear part of the Hamiltonian of the system in the exciton-photon basis can be diagonalized by means of a unitary transformation, introducing polariton modes $\hat{P}_{ln}^\dagger \equiv \hat{P}_\varkappa^\dagger$ as linear combination of excitons and photons. The total Hamiltonian in the polariton basis reads:

$$\hat{H}_{\text{tot}} = \sum_{l=-\infty}^{+\infty} \left\{ \sum_{n=1}^{N(l)} \hbar \omega_{ln} \hat{a}_{ln}^\dagger \hat{a}_{ln} + \sum_{\nu=1}^{+\infty} \hbar \Omega_{l\nu} \hat{X}_{l\nu}^\dagger \hat{X}_{l\nu} + \sum_{n,\nu} \hbar (f_{l\nu n} \hat{X}_{l\nu}^\dagger \hat{a}_{ln} + \text{h.c.}) \right\} + \hat{H}_{\text{xx}} \quad (16)$$

$$= \sum_{\varkappa} \hbar \varepsilon_{\varkappa} \hat{P}_{\varkappa}^\dagger \hat{P}_{\varkappa} + \frac{1}{2} \sum_{\varkappa_1 \varkappa_2 \varkappa_3 \varkappa_4} W_{\varkappa_1 \varkappa_2 \varkappa_3 \varkappa_4} \hat{P}_{\varkappa_1}^\dagger \hat{P}_{\varkappa_2}^\dagger \hat{P}_{\varkappa_3} \hat{P}_{\varkappa_4}, \quad (16')$$

where we used the notations $|\varkappa\rangle \equiv |l(\varkappa), n(\varkappa)\rangle \equiv |l, n\rangle$ or simply $|l\rangle$ (where relevant) to label different polaritonic states. All the mathematical details, together with explicit expressions connecting $V_{\kappa_1 \kappa_2 \kappa_3 \kappa_4}$ with $W_{\varkappa_1 \varkappa_2 \varkappa_3 \varkappa_4}$ are provided in Appendix C.

D. Polaritons dynamics

The system of interacting polaritons can serve as a playground to examine the nonlinear dynamics in the regime of coherent optical pump.

In the mean-field approximation, the Heisenberg equation for the operators \hat{P}_\varkappa can be transformed into the equation of

motion for the the coherent amplitudes $c_\varkappa = \langle \hat{P}_\varkappa \rangle$ which reads:

$$\dot{c}_\varkappa = - \left(i\varepsilon_\varkappa + \frac{\gamma}{2} \right) c_\varkappa - \frac{i\mathcal{S}_\varkappa}{\hbar} \exp(-i\varepsilon_\varkappa t) - \frac{i}{2\hbar} \sum W_{\varkappa_1 \varkappa_2 \varkappa_3 \varkappa_4} (\delta_{\varkappa_1, \varkappa} c_{\varkappa_2}^* + \delta_{\varkappa_2, \varkappa} c_{\varkappa_1}^*) c_{\varkappa_3} c_{\varkappa_4}. \quad (17)$$

Here, we have neglected quantum correlations and used the approximation $\langle \hat{P}_{\varkappa_j}^\dagger \hat{P}_{\varkappa_m} \hat{P}_{\varkappa_s} \rangle = c_{\varkappa_j}^* c_{\varkappa_m} c_{\varkappa_s}$.⁶⁶ The variables \mathcal{S}_\varkappa and γ indicate an amplitude of the \varkappa state coherent pumping and polariton decay rate, respectively. The latter is supposed to be the same for all polaritonic states.

An example of minimal set of states that can demonstrate, under the zero initial conditions, the redistribution of the polaritons between different states is

$$|1\rangle + |1\rangle \leftrightarrow |2\rangle + |0\rangle, \quad (18)$$

which corresponds to the channel with angular momentum transfer of $\Delta l = 1$.

III. RESULTS AND DISCUSSION

For all the calculations, the following cavity parameters were accepted: the micropillar material is GaAs with high-frequency dielectric permittivity $\varepsilon_1 = 10.89$ and the static one $\varepsilon_{\text{st}} = 12.9$, the cylinder radius $R = 1.5 \mu\text{m}$, the effective inter-DBRs distance $L = 134.5 \text{ nm}$, the 2D Rabi splitting (twice the Rabi energy) $\hbar\Omega_{2\text{D}} = 3.2 \text{ meV}$, the polariton linewidth $\hbar\gamma = 70 \mu\text{eV}$. These parameters correspond to the experimental configuration of the reference 13. The effective micropillar height, L , has been varied to get the different values of the detuning between photonic and excitonic modes, and has been finally adjusted to match the resonant case when the lower

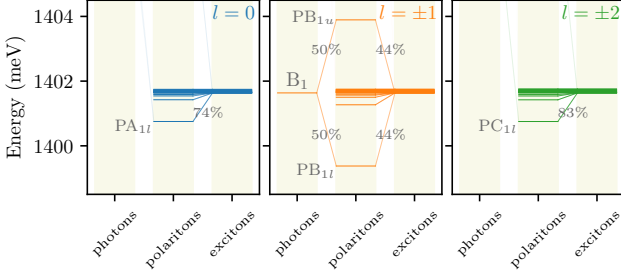


FIG. 3. The lower polaritons formation scheme (for the states around the excitonic resonance, the magnified section of Fig. 2). The states PA_{1l} , PB_{1l} , and PC_{1l} are the lowest polaritonic states with $l = 0, \pm 1$, and ± 2 , respectively. The PB_{1u} state is the counterpart to PB_{1l} one: photonic mode B_1 splits into them almost equally. The percentage fractions present the absolute values of the corresponding Hopfield coefficients, squared.

photonic mode energy (B_1) equals the energy of $1s$ exciton. This condition resulted in $L = 134.5$ nm.

Figure 2 demonstrates both the dependencies of the photonic target function (PTF) on the energy (left parts at each panel) and the hybridization diagram of the exciton-polariton formation for $l = 0, \pm 1, \pm 2$. The numerically determined roots of the PTFs (which give the photonic eigenenergies) are shown by the grey rounds, the horizontal dashed lines explicitly connect them with the corresponding photon levels at the diagrams. The calculations have yielded the total amount of 10, 10, and 8 photonic modes for $|l| = 0, 1$ and 2, respectively (the higher photonic modes are not displayed in the Figure (the energy axis is truncated by the value 1450 meV from the top)).

Fig. 3 presents the zoomed in sections of Fig. 2 outlined by the grey rectangles and illustrates the scheme of polaritons formation in more detail. The states PA_{1l} , PB_{1l} , and PC_{1l} are the lowest polaritonic states with $l = 0, \pm 1$, and ± 2 , respectively. The percent values display the Hopfield coefficients, e.g. the two 50% marks near photonic state B_1 mean that the latter splits into polaritonic states PB_{1u} and PB_{1l} in equal proportions (the separation energy equals 4.52 meV which is 1.4 times greater than $\hbar\Omega_{2D}$).

Each photonic mode with a given angular momentum, l , generally couples with the whole infinite set of excitonic states with $\lambda=l$. This gives rise, firstly, to the infinite number of polaritons with the identical l , and secondly, to the infinite number of terms in the excitons-over-polaritons decomposition used to calculate the $\tilde{W}_{\kappa_1 \kappa_2 \kappa_3 \kappa_4}$ via $\tilde{V}_{\kappa_1 \kappa_2 \kappa_3 \kappa_4}$. On the other hand, some of the HCs are negligibly small, which is used to truncate the infinite-length decompositions, see Appendix E for details.

The exciton-exciton interaction coefficients $V_{\kappa_1 \kappa_2 \kappa_3 \kappa_4}$ are defined via the 8-dimensional integral (10d) and have been computed by virtue of the Monte-Carlo integration algorithm (utilizing both the importance and uniform random samplings). The number of integrand evaluations was regulated by the maximal sufficient absolute error of $0.01 \mu\text{eV}$. Also as V_C has a $1/r$ singularity, necessary changes of variables have

been performed to integrate each summand of $V_{\text{int},xx}$ (10c) in (10d). The real parts

$$\tilde{V}_{n_1 n_2} \equiv \Re V_{1,n_1;1,n_2;2,n_2;0,n_1} \quad (19)$$

for $n_1, n_2 = 1, \dots, 5, 11, \dots, 15$ are presented in Figure 4(A), the numeric data are gathered in Table D1.

The polariton-polariton interaction matrix elements

$$\tilde{W}_{n_1 n_2} \equiv |W_{1,n_1;1,n_2;2,n_2;0,n_1}| \quad (20)$$

for the same set of n_1 and n_2 have been then evaluated via the sums (C2b), and are presented in Figure 4(B) and Table D2. Figure 4(C) completes the picture with the difference $|\tilde{W}_{n_1 n_2}| - |\tilde{V}_{n_1 n_2}|$.

Each of the panels in Fig. 4 is divided into four quadrants in accordance with the groups of numbers n_1 and n_2 . The transitions from panel (A) to (B) and (C) is quantitatively distinct for different quadrants. The ranges (1...5) and (11...15) principally differ by the values of HCs performing the transition from $V_{\kappa_1 \kappa_2 \kappa_3 \kappa_4}$ to $W_{\kappa_1 \kappa_2 \kappa_3 \kappa_4}$, see (E1) and (E2): for the latter range the corresponding HCs absolute values are almost equal to unity. That is why $|\tilde{W}_{n_1, n_2}| \approx |\tilde{V}_{n_1, n_2}|$ when $n_1, n_2 \gtrsim 10$, which is clearly seen by the white coloured area in Fig. 4(C).

The dynamics of the micropillar polaritons (17) was studied in more detail for the system consistent of five interacting polaritonic states subject to partial coherent pumping (PCP). The states are $|0\rangle$, $|\pm 1\rangle$, and $|\pm 2\rangle$ with the fixed $n_j = 1$, their eigenenergies - $\hbar\epsilon_{0,1} = 1400.752$ meV, $\hbar\epsilon_{\pm 1,1} = 1399.376$ meV, and $\hbar\epsilon_{\pm 2,1} = 1400.751$ meV (the data are put down with that precision as the interaction matrix elements are of μeV order of magnitude). The states are PA_{1l} , PB_{1l} , and PC_{1l} in Fig. 3, their excitonic parts wave functions are the purple surfaces on the right panel of Fig. 1. For the system considered, there are 85 nontrivial matrix elements $W_{\kappa_1 \kappa_2 \kappa_3 \kappa_4}$ that meet the angular momentum conservation law (see Appendix F), their absolute values vary from 0.35 to $1.34 \mu\text{eV}$. The model decay rate $\hbar\gamma = 70 \mu\text{eV}^{13}$ corresponds to a lifetime $\tau \approx 59$ ps. The zero initial conditions Cauchy problem was numerically integrated by means of the classic Runge-Kutta method with an invariant step of ca. 5 fs.

Figures 5(A), (B), and (C) exhibit the dynamics of the states populations ($|c_0(t)|^2$, $|c_1(t)|^2 + |c_{-1}(t)|^2$, and $|c_2(t)|^2 + |c_{-2}(t)|^2$), panel (D) shows the phase trajectory of the dynamics (C). The states are coherently pumped under the following schemes: (1) $S_0^{(1)} = 0, S_1^{(1)} = S_{-1}^{(1)} = S_2^{(1)} = S_{-2}^{(1)} = S/\sqrt{2}$ (panel A), (2) $S_0^{(2)} = S, S_1^{(2)} = S_{-1}^{(2)} = S/\sqrt{2}, S_{\pm 2}^{(2)} = 0$ (panel B), and (3) $S_0^{(3)} = 0.2S, S_1^{(3)} = -S_{-1}^{(3)} = 0.2S/\sqrt{2}, S_{\pm 2}^{(3)} = 0$ (panels C and D), with common notation $S = 40$ meV.

The results for the schemes (1) and (2) demonstrate several similar features: i) the populations swing around close corresponding values, ii) both limit trajectories are limit cycles (not shown here) which are the line segments due to the phase synchronization of the vibrating populations, iii) the long-range periods $\tau^{(1)} \approx \tau^{(2)} \approx 19$ ps, iv) the states arranged in ascending order by the overall populations (at distant times) are $|\pm 2\rangle$,

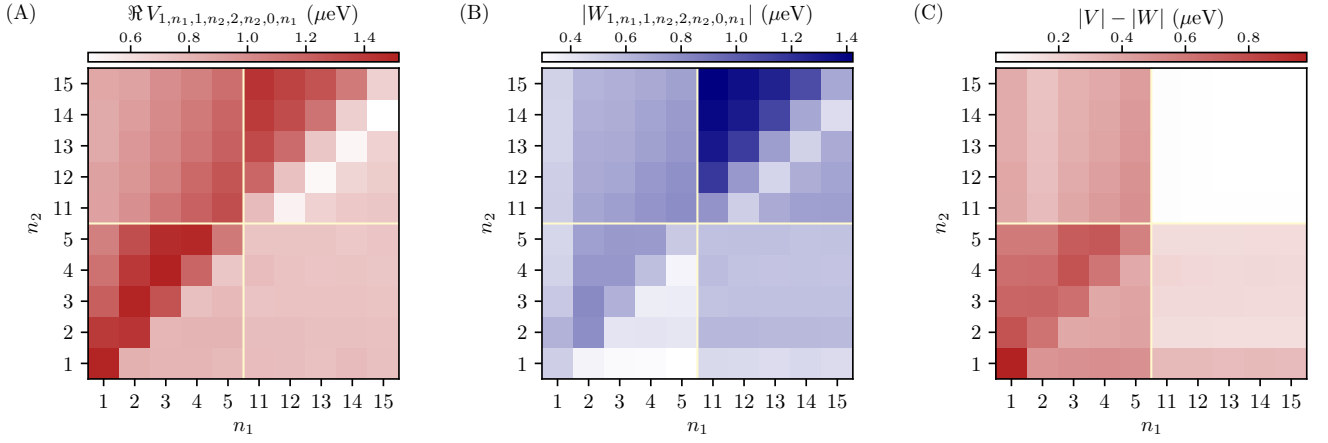


FIG. 4. The absolute values of (A) exciton-exciton, $V_{\kappa_1 \kappa_2 \kappa_3 \kappa_4}$, and (B) polariton-polariton, $W_{\varkappa_1 \varkappa_2 \varkappa_3 \varkappa_4}$, interaction matrix elements, and (C) their difference, $|V| - |W|$. All the V s and W s are measured in μeV . The states examined are $\kappa_1 = \varkappa_1 = (1, n_1)$, $\kappa_2 = \varkappa_2 = (1, n_2)$, $\kappa_3 = \varkappa_3 = (2, n_2)$, $\kappa_4 = \varkappa_4 = (0, n_1)$, with integers $n_1, n_2 = 1, \dots, 5, 11, \dots, 15$. The essence of the colour schemes used for all the panels is common: the associated absolute values grow with the increase in the colour saturation. The horizontal colour bars show the scales.

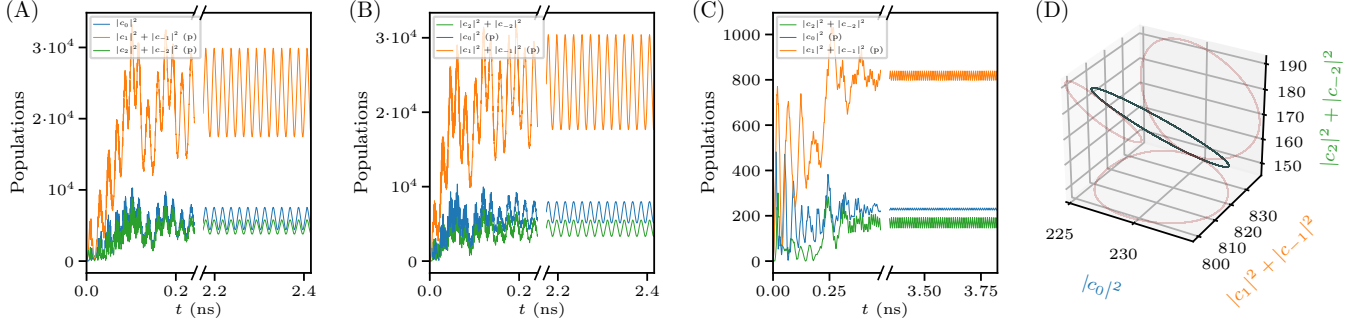


FIG. 5. (A, C) The populations dynamics of the system consistent of the five polaritonic states: $|c_0(t)|^2$ (blue lines), $|c_1(t)|^2 + |c_{-1}(t)|^2$ (red lines), and $|c_2(t)|^2 + |c_{-2}(t)|^2$ (green lines), where the indices stand for the angular momenta. The lowest polaritonic modes ($n_l=1$) are taken for all l . The time axis is broken to show both the transient period and the periodic behaviour. (B, D) The phase trajectories (the limit cycles here; black solid lines for the later times (right parts in (A, C))). The states with (A, B) $l = \pm 1, \pm 2$, and (C, D) $l = 0, \pm 1$ are coherently pumped, which is marked by (p) in the legends. The semi-transparent red curves are the projections onto the coordinate planes.

$|0\rangle$, and $|\pm 1\rangle$. On the other hand, this order can be treated as inverse for the scheme (1) as soon as state $|0\rangle$ is not directly pumped and, nevertheless, its population (averaged over the limit period) exceeds that of the pair of pumped states, $|\pm 2\rangle$, see Fig. 5(B).

Scheme (3) differs from (1) and (2) as it assumes the possibility to control the phase of the pumping field for the states with similar energies and distinct angular momenta. In the calculation, the pumping fields for $|+1\rangle$ and $|-1\rangle$ states have the same amplitudes and the phase shift of π . The limit cycle in the case acquires a pronounced oval shape.

These results demonstrate, that the system can be regarded as a source of photons carrying angular momenta different from those which are directly excited by the coherent pumping.

IV. CONCLUSION

We considered theoretically the formation of exciton-

polaritons in cylindric micropillars, their interaction, and pump-loss dynamics. The exciton-exciton interaction matrix elements were numerically computed by means of the Monte-Carlo integration algorithm and converted to polariton-polariton ones through the unitary transformation. To analyze the nonlinear optical dynamics, we utilized the Heisenberg equation for the polaritonic operators and applied the mean-field truncation scheme which allowed us to study the effect of the nonlinear redistribution of the polariton between different confined modes. Our results can form a basis for the realization of a source of photons carrying non-zero orbital angular momenta.

ACKNOWLEDGMENTS

The work was supported by Priority 2030 Federal Academic Leadership Program. I.A.S. acknowledges support from the Icelandic Research Fund (Project "Hybrid polariton-

ics").

Appendix A: Cavity photonic modes

As described above, the microcavity is placed between the pair of DBRs and contains the cylindric micropillars of radius R with the high-frequency dielectric permittivity ϵ_1 . The effective inter-DBRs distance is denoted as L . In this geometry, the z -components of the electric field inside the micropillar (core region, index 1) and outside it (air region, index 2) are sought in the form

$$E_z^{(1)}(r, \theta, z, t) = A_l J_l(\beta_1 r) \cos \alpha z \exp i(l\theta - \omega t), \quad (\text{A1a})$$

$$E_z^{(2)}(r, \theta, z, t) = C_l K_l(\beta_2 r) \cos \alpha z \exp i(l\theta - \omega t), \quad (\text{A1b})$$

where J_l and K_l are l -th order Bessel's functions of the first and second kind, respectively, and $\alpha = \pi/L$ gives the fundamental mode in z -direction.

The condition of the fields tangential components continuity at the core-to-vacuum boundary ($r = R$) leads to the following characteristic equation:

$$l^2 \cdot \alpha^2 \cdot \left(\frac{1}{u^2} + \frac{1}{v^2} \right)^2 = (\eta_1 + \eta_2) (k_1^2 \eta_1 + k_2^2 \eta_2), \quad (\text{A2})$$

and the corresponding target function presented in the main text.

The frequencies ω_{ln} being determined, one then gets the electric field projections in the core region:

$$E_{ln,z}(\mathbf{r}) = \cos \alpha z \cdot e^{il\theta} \cdot A_{ln} \cdot J_l(x), \quad (\text{A3a})$$

$$E_{ln,r}(\mathbf{r}) = \cos \alpha z \cdot e^{il\theta} \cdot A_{ln} \cdot \frac{i\alpha}{\beta_1} \cdot \left[J_l'(x) - l^2 \alpha_{ln} \frac{J_l(x)}{x} \right], \quad (\text{A3b})$$

$$E_{ln,\theta}(\mathbf{r}) = \cos \alpha z \cdot e^{il\theta} \cdot A_{ln} \cdot \frac{\alpha l}{\beta_1} \cdot \left[J_l'(x) \alpha_{ln} - \frac{J_l(x)}{x} \right], \quad (\text{A3c})$$

where $x = \beta_1 r$, and

$$\alpha_{ln} = J_l(u) \cdot \left(\frac{1}{u^2} + \frac{1}{v^2} \right) \cdot \left(\frac{J_l'(u)}{u} + \frac{K_l'(v) J_l(u)}{K_l(v) v} \right)^{-1}. \quad (\text{A4})$$

To get the temporal dependence, one is to multiply equations (A3) by $e^{-i\omega_{ln}t}$. To obtain the fields in the outer region, the amplitude A_{ln} should be swapped for C_{ln} , β_1 for β_2 , BFs of the first kind J_l – for the BFs of the second kind K_l , and their argument should be changed to $x = \beta_2 r$. The multiple subscript index ln has been attached to α because of the implicit dependence of u and v on both l and n via $\beta_{1,2}$ (3c). The prefactors A and C (see eqs. (A1)) also acquire both indices: A_{ln} and C_{ln} .

To get the constant A_{ln} , we normalize the electric field by the energy of a single photon^{67,68}:

$$\hbar \omega_{ln} = \epsilon_0 \iiint_{\text{MC}} \epsilon(\mathbf{r}) |\mathbf{E}_{ln}(\mathbf{r})|^2 d^3 \mathbf{r} = A_{ln}^2 G_{ln} \Rightarrow A_{ln} = \sqrt{\frac{\hbar \omega_{ln}}{G_{ln}}}. \quad (\text{A5})$$

The integration is carried over the whole cavity volume, the dependence of the high-frequency permittivity on the position is denoted via $\epsilon(\mathbf{r})$ which equals ϵ_1 inside the micropillar and unity outside. The normalization constant is calculated as

$$G_{ln} = \epsilon_0 \pi^2 \alpha \cdot \left\{ \frac{\epsilon_1}{\beta_1^4} \int_0^u x dx \left[(1 + l^2 \alpha_{ln}^2) \left(J_l'^2(x) + \frac{l^2 J_l^2(x)}{x^2} \right) + \frac{\beta_1^2}{\alpha^2} J_l^2(x) \right] + \frac{1}{\beta_2^4} \int_v^{+\infty} x dx \left[(1 + l^2 \alpha_{ln}^2) \left(K_l'^2(x) + \frac{l^2 K_l^2(x)}{x^2} \right) + \frac{\beta_2^2}{\alpha^2} K_l^2(x) \right] \left(\frac{J_l(u)}{K_l(v)} \right)^2 + 2l^2 \alpha_l J_l^2(u) \left(\frac{1}{\beta_2^4} - \frac{\epsilon_1}{\beta_1^4} \right) \right\}. \quad (\text{A6})$$

The parameter α_{ln} is determined in (A4). The integration is carried on over the quantum well ($0 \leq x \leq u$) and over the outer region ($x \geq v$).

Appendix B: Exciton-photon coupling

Recall eq. (14) for the exciton-photon interaction amplitude and extend it by inserting the expressions for the excitonic overlap wave function $\Phi_{\lambda\nu}$ (7a) and the electric field (A3), and integrating out the angular dependence $e^{i\theta(l-\lambda)}$:

$$\hbar g_{ln\lambda\nu} = -\chi_{1s}(0) \iint_{\text{QW}} \Phi_{\lambda\nu}(\mathbf{r}) [\mathbf{d}_{\text{cv}}(\mathbf{r}) \cdot \mathbf{E}_{ln}(\mathbf{r})]_{z=0} d^2\mathbf{r} = -\frac{d_{\text{cv}}\chi_{1s}(0)}{\sqrt{2}} \iint_{\text{QW}} \Phi_{\lambda\nu}(\mathbf{r}) [E_{ln,r}(\mathbf{r}) + iE_{ln,\theta}(\mathbf{r})]_{z=0} d^2\mathbf{r} \quad (\text{B1})$$

$$= -i\delta_{l\lambda} d_{\text{cv}}\chi_{1s}(0) \sqrt{\frac{2\hbar\omega_{ln}}{G_{ln}}} \frac{\varkappa\pi}{\beta_1 |J_{|\lambda|+1}|(x_{\lambda\nu})} \int_0^R r dr J_\lambda(\alpha_{\lambda\nu} r) \left\{ \left[J'_l(x) - l^2 \alpha_{ln} \frac{J_l(x)}{x} \right] + l \left[J'_l(x) \alpha_{ln} - \frac{J_l(x)}{x} \right] \right\} \quad (\text{B2})$$

$$\equiv \hbar f_{l\nu n} \delta_{l\lambda}, \quad (\text{B3})$$

where $x = \beta_1 r$.

To make the theory uniform and utilize the experimental data for obtaining d_{cv} , we also derive the Rabi splitting for a square-shaped quantum well within the same formalism. In this case, the photonic field is given by

$$\mathbf{E}_{\mathbf{k}}(\mathbf{r}) = e_p A_{\mathbf{k}} \cos \varkappa z e^{i\mathbf{k}r_{\parallel}}, \quad (\text{B4})$$

where \varkappa carries the same meaning as earlier, \mathbf{k} is the in-plane (xy) quasimomentum, e_p is the polarization unit vector, r_{\parallel} is the in-plane radius-vector, $A_{\mathbf{k}}$ is the normalization constant which is defined via

$$\hbar\omega_{\mathbf{k}} = \varepsilon_0 \int_{\text{MC}} \varepsilon(\mathbf{r}) |\mathbf{E}_{\mathbf{k}}(\mathbf{r})|^2 d^3\mathbf{r} = A_{\mathbf{k}}^2 \frac{\varepsilon_0 \varepsilon L S}{2} \Rightarrow A_{\mathbf{k}} = \sqrt{\frac{2\hbar\omega_{\mathbf{k}}}{\varepsilon_0 \varepsilon L S}}. \quad (\text{B5})$$

Here, S is the lateral square of the rectangular shaped microcavity (coinciding with the QW square). The excitonic overlap function (for the centre of mass motion) is

$$\Phi_{\mathbf{k}}(r_{\parallel}) = \frac{e^{i\mathbf{k}r_{\parallel}}}{\sqrt{S}} \quad (\text{B6})$$

with the same normalization area S . Therefore, the exciton-photon interaction amplitude is

$$\hbar g_{\mathbf{k}\mathbf{k}'} = -\chi_{1s}(0) (\mathbf{d}_{\text{cv}} \cdot e_p) \sqrt{\frac{2\hbar\omega_{\mathbf{k}}}{\varepsilon_0 \varepsilon L S^2}} \iint_{\text{QW}} e^{i\mathbf{r}_{\parallel}(\mathbf{k}-\mathbf{k}')} dx dy = -\chi_{1s}(0) d_{\text{cv}} \frac{e_{p,x} + i e_{p,y}}{\sqrt{2}} \sqrt{\frac{2\hbar\omega_{\mathbf{k}}}{\varepsilon_0 \varepsilon L}} \delta_{\mathbf{k}\mathbf{k}'}. \quad (\text{B7})$$

The presence of $\delta_{\mathbf{k}\mathbf{k}'}$ indicates the coupling of the excitons and photons with the same in-plane quasimomenta.

The Rabi splitting, $\hbar\Omega_{2\text{D}}$, equals twice the amplitude (its absolute value) (B7) for the case $\hbar\omega_{\mathbf{k}} = \hbar\Omega_x$:

$$\hbar\Omega_{2\text{D}} = 2\chi_{1s}(0) d_{\text{cv}} \sqrt{\frac{\hbar\Omega_x}{\varepsilon_0 \varepsilon L}}. \quad (\text{B8})$$

Hence,

$$\chi_{1s}(0) d_{\text{cv}} = \frac{\hbar\Omega_{2\text{D}}}{2} \sqrt{\frac{\varepsilon_0 \varepsilon L}{\hbar\Omega_x}}, \quad (\text{B9})$$

which is used in the main text, see Section II C.

Appendix C: Transition to polaritonic basis

Recall eqs. (16) and (16') for the total Hamiltonian:

$$\hat{H}_{\text{tot}} = \sum_{l=-\infty}^{+\infty} \left\{ \sum_{n=1}^{N(l)} \hbar\omega_{ln} \hat{a}_{ln}^{\dagger} \hat{a}_{ln} + \sum_{\nu=1}^{+\infty} \hbar\Omega_{l\nu} \hat{X}_{l\nu}^{\dagger} \hat{X}_{l\nu} + \sum'_{n,\nu} \hbar (f_{l\nu n} \hat{X}_{l\nu}^{\dagger} \hat{a}_{ln} + \text{h.c.}) \right\} + \hat{H}_{\text{xx}} \quad (\text{16})$$

$$= \sum_{\varkappa} \hbar \varepsilon_{\varkappa} \hat{P}_{\varkappa}^{\dagger} \hat{P}_{\varkappa} + \frac{1}{2} \sum_{\varkappa_1 \varkappa_2 \varkappa_3 \varkappa_4} W_{\varkappa_1 \varkappa_2 \varkappa_3 \varkappa_4} \hat{P}_{\varkappa_1}^{\dagger} \hat{P}_{\varkappa_2}^{\dagger} \hat{P}_{\varkappa_3} \hat{P}_{\varkappa_4}. \quad (16')$$

The first three terms in (16) form linear part of the total Hamiltonian. This part can be reduced to the diagonal form in the basis of polaritonic operators, $\hat{P}_{ln}^{\dagger} \equiv \hat{P}_{\varkappa}^{\dagger}$, by a unitary transformation, thus giving the first sum in (16'). As only the excitons and photons with same angular momenta are coupled, one can write this transformation in the form

$$\hat{P}_{ln} = \sum B_{l,n\nu} \hat{X}_{l\nu} + \sum C_{l,nn'} \hat{a}_{ln'}, \quad \hat{X}_{l\nu} = A_{l,\nu n} \hat{P}_{ln} \quad (C1a)$$

or shortly

$$\hat{P}_{\varkappa} = \sum_{\kappa} B_{\varkappa\kappa} \hat{X}_{\kappa} + \sum_k C_{\varkappa k} \hat{a}_k, \quad \hat{X}_{\kappa} = \sum_{\varkappa} A_{\varkappa\varkappa} \hat{P}_{\varkappa}, \quad (C1b)$$

keeping in mind that $l(\varkappa) = l(k) = \lambda(\kappa)$. Here, $B_{\kappa k}$, $C_{\varkappa k}$, and $A_{\varkappa\varkappa}$ are the 4-index matrices of the Hopfield coefficients of the direct (B , C) and inverse (A) unitary transformations, respectively.

The exciton-exciton interaction term, \hat{H}_{xx} (2d), can be rewritten in the polariton basis which leads to the polariton-polariton interaction:

$$\hat{H}_{xx} \equiv \hat{H}_{pp} = \frac{1}{2} \sum_{\varkappa_1 \varkappa_2 \varkappa_3 \varkappa_4} W_{\varkappa_1 \varkappa_2 \varkappa_3 \varkappa_4} \hat{P}_{\varkappa_1}^{\dagger} \hat{P}_{\varkappa_2}^{\dagger} \hat{P}_{\varkappa_3} \hat{P}_{\varkappa_4}, \quad (C2a)$$

where

$$W_{\varkappa_1 \varkappa_2 \varkappa_3 \varkappa_4} = \sum'_{\kappa_1 \kappa_2 \kappa_3 \kappa_4} A_{\kappa_1 \varkappa_1} A_{\kappa_2 \varkappa_2} A_{\kappa_3 \varkappa_3} A_{\kappa_4 \varkappa_4} V_{\kappa_1 \kappa_2 \kappa_3 \kappa_4}. \quad (C2b)$$

is the corresponding matrix element. Formally, matrices A are of infinite size as there are infinite number of excitons possessing each angular momentum λ (and hence there are the infinite number of polaritons for each l). Therefore, each sum in (C1b) is formally of infinite length, which is overcome by a truncation, see Appendix E.

Appendix D: Exciton-exciton and polariton-polariton interaction matrix elements

In what follows, real parts of the exciton-exciton interaction matrix elements ($\tilde{V}_{n_1 n_2}$)

15	0.88	0.90	1.0	1.06	1.15	1.43	1.36	1.28	1.09	0.68
14	0.86	0.92	1.02	1.09	1.20	1.40	1.31	1.12	0.69	0.45
13	0.86	0.95	1.04	1.12	1.22	1.33	1.17	0.73	0.5	0.68
12	0.91	0.96	1.06	1.18	1.27	1.19	0.76	0.49	0.66	0.70
11	0.91	0.99	1.12	1.21	1.31	0.78	0.52	0.68	0.72	0.73
5	1.07	1.31	1.47	1.49	1.10	0.74	0.74	0.74	0.72	0.73
4	1.14	1.41	1.52	1.2	0.73	0.78	0.75	0.73	0.74	0.73
3	1.23	1.51	1.29	0.76	0.79	0.74	0.75	0.75	0.75	0.74
2	1.40	1.42	0.80	0.82	0.82	0.77	0.77	0.76	0.76	0.75
1	1.50	0.83	0.82	0.81	0.79	0.78	0.77	0.75	0.78	0.76
$\uparrow n_2/n_1 \rightarrow$	1	2	3	4	5	11	12	13	14	15

and the polariton-polariton ones ($\tilde{W}_{n_1 n_2}$)

15	0.50	-0.63	0.65	-0.68	0.71	1.42	-1.35	1.27	-1.09	0.68
14	-0.49	0.65	-0.66	0.70	-0.74	-1.39	1.30	-1.12	0.68	-0.45
13	0.49	-0.67	0.67	-0.71	0.76	1.32	-1.16	0.73	-0.50	0.67
12	0.52	-0.67	0.68	-0.75	0.79	1.17	-0.75	0.49	-0.66	0.70
11	-0.52	0.69	-0.72	0.77	-0.81	-0.77	0.51	-0.67	0.72	-0.72
5	0.48	-0.71	0.75	-0.74	0.53	0.58	-0.58	0.58	-0.56	0.57
4	0.50	-0.76	0.75	-0.59	0.35	0.59	-0.57	0.56	-0.57	0.56
3	-0.54	0.82	-0.65	0.38	-0.38	-0.57	0.58	-0.58	0.58	-0.58
2	0.64	-0.80	0.42	-0.42	0.41	0.61	-0.61	0.61	-0.61	0.60
1	-0.51	0.35	-0.32	0.31	-0.30	-0.47	0.46	-0.45	0.47	-0.46
$\uparrow n_2/n_1 \rightarrow$	1	2	3	4	5	11	12	13	14	15

are presented. All the values are given in μeV . The imaginary parts are omitted as soon as their maximal absolute values are $0.01 \mu\text{eV}$ and $0.001 \mu\text{eV}$ for $\tilde{V}_{n_1 n_2}$ and $\tilde{W}_{n_1 n_2}$, respectively. The sections of (D1) and (D2) highlighted by the bold font are the ranges with close resemblance between the absolute values of $\tilde{V}_{n_1 n_2}$ and $\tilde{W}_{n_1 n_2}$. These areas form the upper-right quadrant in Fig. 4(C) which is almost white as the associated difference is vanishingly small. The values $\tilde{V}_{n_1 n_2}$ have been calculated with the accuracy of $0.01 \mu\text{eV}$.

Appendix E: Truncating the excitons-over-polaritons decompositions

The infinite-length decompositions of the excitons addressed in the main text and in Appendix C lead to each sum for $W_{\kappa_1 \kappa_2 \kappa_3 \kappa_4}$ (C2b) to be formally of the infinite length as well. To overcome it, we have, firstly, limited the number of excitonic modes (by 20 which is twice the maximal number of photonic modes with a fixed $|l| \leq 2$). Secondly, we have truncated the decompositions of excitonic operators \hat{X}_κ (C1b) keeping only the summands with $\mathcal{A}_{\kappa \kappa'}$ greater than half the achievable maximum in the row: if $|\mathcal{A}_{\kappa \kappa'}| \geq 0.5 \max |\mathcal{A}_{\kappa \kappa''}|$ with the condition that the maximum is not less than 0.1 (actually, it was satisfied for all the states – there is no excitonic state with all the HCs less than 0.1).

For the excitonic states under the study, the operators can be schematically put down as

$$\begin{aligned} \hat{X}_{0,1} &\simeq 0.86i\hat{P}_{0,1}; & \hat{X}_{0,2} &\simeq 0.82i\hat{P}_{0,2}; & \hat{X}_{0,3} &\simeq 0.77i\hat{P}_{0,3}; & \hat{X}_{0,4} &\simeq -0.75i\hat{P}_{0,4}; & \hat{X}_{0,5} &\simeq 0.74i\hat{P}_{0,5}; \\ \hat{X}_{1,1} &\simeq 0.66i\hat{P}_{1,1} + 0.66i\hat{P}_{1,21}; & \hat{X}_{1,2} &\simeq -0.85i\hat{P}_{1,2}; & \hat{X}_{1,3} &\simeq 0.84i\hat{P}_{1,3}; & \hat{X}_{1,4} &\simeq 0.85i\hat{P}_{1,4}; & \hat{X}_{1,5} &\simeq 0.84i\hat{P}_{1,5}; \\ \hat{X}_{2,1} &\simeq -0.91i\hat{P}_{2,1}; & \hat{X}_{2,2} &\simeq -0.94i\hat{P}_{2,2}; & \hat{X}_{2,3} &\simeq -0.92i\hat{P}_{2,3}; & \hat{X}_{2,4} &\simeq 0.90i\hat{P}_{2,4}; & \hat{X}_{2,5} &\simeq 0.93i\hat{P}_{2,5}. \end{aligned} \quad (\text{E1})$$

As seen, all the HCs are purely imaginary (which is valid for all other states as well). For $n \geq 11$, the absolute value of HC between $\hat{X}_{l,n}$ and $\hat{P}_{l,n}$ equals unity with the accuracy $\sim 10^{-2}$.

Under the conditions, each of the sums (C2b) is reduced to a single term:

$$W_{\kappa_1 \kappa_2 \kappa_3 \kappa_4} = \mathcal{A}_{\kappa_1 \kappa_1} \mathcal{A}_{\kappa_2 \kappa_2} \mathcal{A}_{\kappa_3 \kappa_3} \mathcal{A}_{\kappa_4 \kappa_4} V_{\kappa_1 \kappa_2 \kappa_3 \kappa_4}. \quad (\text{E2})$$

Due to the purely imaginary (for each $\mathcal{A}_{\kappa \kappa}$) and real (for $V_{\kappa_1 \kappa_2 \kappa_3 \kappa_4}$) structures, the matrix elements $W_{\kappa_1 \kappa_2 \kappa_3 \kappa_4}$ are also real, which is seen in (D2) and (F1).

Appendix F: $W_{\kappa_1 \kappa_2 \kappa_3 \kappa_4}$ matrix elements for the dynamics calculations

As mentioned in the main text, there are totally 85 nontrivial $W_{\kappa_1 \kappa_2 \kappa_3 \kappa_4}$ coefficients for scattering among $|0\rangle$, $|\pm 1\rangle$ and $|\pm 2\rangle$ polaritonic states (with all $n(\kappa_j)=0$). For the sake of brevity, we shrink the indices $\kappa_1 \kappa_2 \kappa_3 \kappa_4$ to the lists (l_1, l_2, l_3, l_4) and put down the W -values:

$$\begin{aligned} W_{0,0,0,0} &= 1.342 \mu\text{eV}, \\ W_{-2,2,2,-2} &= W_{2,-2,2,-2} = W_{-2,2,-2,2} = W_{2,-2,-2,2} = 1.228 \mu\text{eV}, \\ W_{2,2,2,2} &= W_{-2,-2,-2,-2} = 1.226 \mu\text{eV}, \\ W_{0,-2,0,-2} &= W_{0,2,2,0} = W_{2,0,2,0} = W_{-2,0,-2,0} = W_{2,0,0,2} = W_{-2,0,0,-2} = W_{0,2,0,2} = W_{0,-2,-2,0} = 0.769 \mu\text{eV}, \\ W_{0,0,-2,2} &= W_{0,0,2,-2} = 0.768 \mu\text{eV}, \\ W_{2,-2,0,0} &= W_{-2,2,0,0} = 0.763 \mu\text{eV}, \\ W_{-1,-2,-2,-1} &= W_{-1,-2,-1,-2} = W_{1,2,2,1} = W_{-2,-1,-1,-2} = W_{1,2,1,2} = W_{2,1,1,2} = W_{2,1,2,1} = W_{-2,-1,-2,-1} = 0.622 \mu\text{eV}, \\ W_{2,-2,-1,1} &= W_{-2,2,-1,1} = W_{2,-2,1,-1} = W_{-2,2,1,-1} = W_{1,-1,2,-2} = W_{-1,1,-2,2} = W_{-1,1,2,-2} = W_{1,-1,-2,2} = -0.613 \mu\text{eV}, \\ W_{1,-2,-2,1} &= W_{-1,2,-1,2} = W_{-1,2,2,-1} = W_{-2,1,-2,1} = W_{2,-1,-1,2} = W_{1,-2,1,-2} = W_{2,-1,2,-1} = W_{-2,1,1,-2} = 0.612 \mu\text{eV}, \\ W_{0,0,-1,1} &= W_{0,0,1,-1} = W_{1,-1,0,0} = W_{-1,1,0,0} = -0.543 \mu\text{eV}, \\ W_{1,0,1,0} &= W_{0,-1,-1,0} = W_{0,1,1,0} = W_{-1,0,0,-1} = W_{-1,0,-1,0} = W_{1,0,0,1} = W_{0,1,0,1} = W_{0,-1,0,-1} = 0.539 \mu\text{eV}, \\ W_{-1,0,-2,1} &= W_{-1,0,1,-2} = W_{0,1,-1,2} = W_{1,0,2,-1} = W_{0,1,2,-1} = W_{0,-1,-2,1} = W_{0,-1,1,-2} = W_{1,0,-1,2} = 0.521 \mu\text{eV}, \\ W_{1,1,2,0} &= W_{1,1,0,2} = W_{-1,-1,-2,0} = W_{-1,-1,0,-2} = -0.516 \mu\text{eV}, \\ W_{-1,2,0,1} &= W_{-1,2,1,0} = W_{1,-2,-1,0} = W_{-2,1,-1,0} = W_{1,-2,0,-1} = W_{2,-1,0,1} = W_{-2,1,0,-1} = W_{2,-1,1,0} = 0.515 \mu\text{eV}, \\ W_{0,-2,-1,-1} &= W_{0,2,1,1} = W_{-2,0,-1,-1} = W_{2,0,1,1} = -0.512 \mu\text{eV}, \\ W_{1,-1,1,-1} &= W_{1,-1,-1,1} = W_{-1,1,-1,1} = W_{-1,1,1,-1} = 0.347 \mu\text{eV}, \\ W_{1,1,1,1} &= W_{-1,-1,-1,-1} = 0.346 \mu\text{eV}. \end{aligned} \quad (\text{F1})$$

- ¹Alexey V Kavokin, Jeremy J Baumberg, Guillaume Malpuech, and Fabrice P Laussy. *Microcavities*. Oxford University Press, 2017.
- ²Iacopo Carusotto and Cristiano Ciuti. Quantum fluids of light. *Rev. Mod. Phys.*, 85:299–366, Feb 2013.
- ³Hui Deng, Hartmut Haug, and Yoshihisa Yamamoto. Exciton-polariton bose-einstein condensation. *Rev. Mod. Phys.*, 82:1489–1537, May 2010.
- ⁴T. Byrnes, N. Kim, and Y. Yamamoto. Exciton-polariton condensates. *Nature Phys.*, 10:803–813, 2014.
- ⁵F. Claude, M. J. Jacquet, R. Usciati, I. Carusotto, E. Giacobino, A. Bramati, and Q. Glorieux. High-resolution coherent probe spectroscopy of a polariton quantum fluid. *Phys. Rev. Lett.*, 129:103601, Aug 2022.
- ⁶J. Kasprzak, M. Richard, S. Kundermann, A. Baas, J. M. J. Jeambrun, P. Keeling, F. M. Marchetti, M. H. Szymanska, R. Andre, J. M. Staehli, V. Savona, P. B. Littlewood, B. Deveaud, and L. Si Dang. Bose-einstein condensation of exciton polaritons. *Nature*, 443:409–414, 2006.
- ⁷R. Balili, V. Hartwell, D. Snoke, and K. West. Bose-einstein condensation of microcavity polaritons in a trap. *Science*, 316:1007–1010, 2007.
- ⁸C. Schneider, A. Rahimi-Iman, N. Y. Kim, J. Fischer, I. G. Savenko, M. Amthor, M. Lerner, A. Wolf, L. Worschech, V. D. Kulakovskii, I. A. Shelykh, M. Kamp, S. Reitzenstein, A. Forchel, Y. Yamamoto, and S. Höfling. An electrically pumped polariton laser. *Nature*, 497:348–352, 2013.
- ⁹F. Riminucci, V. Ardizzone, L. Francaviglia, M. Lorenzon, C. Stavrakas, S. Dhuey, A. Schwartzberg, S. Zanotti, D. Gerace, K. Baldwin, L. N. Pfeiffer, G. Gigli, D. F. Ogletree, A. Weber-Bargioni, S. Cabrini, and D. Sanvitto. Nanostructured GaAs/(Al,Ga)As waveguide for low-density polariton condensation from a bound state in the continuum. *Phys. Rev. Applied*, 18:024039, Aug 2022.
- ¹⁰A. Amo, S. Pigeon, D. Sanvitto, V. G. Sala, R. Hivet, I. Carusotto, F. Pisanello, G. Lemenager, R. Houdre, R. Giacobino, C. Ciuti, and A. Bramati. Polariton superfluids reveal quantum hydrodynamic solitons. *Science*, 332:1167–1170, 2011.
- ¹¹J. K. Chana, M. Sich, F. Fras, A. V. Gorbach, D. V. Skryabin, E. Cancellieri, E. A. Cerda-Méndez, K. Biermann, R. Hey, P. V. Santos, M. S. Skolnick, and D. N. Krizhanovskii. Spatial patterns of dissipative polariton solitons in semiconductor microcavities. *Phys. Rev. Lett.*, 115:256401, Dec 2015.
- ¹²M. Sich, J. K. Chana, O. A. Egorov, H. Sigurdsson, I. A. Shelykh, D. V. Skryabin, P. M. Walker, E. Clarke, B. Royall, M. S. Skolnick, and D. N. Krizhanovskii. Transition from propagating polariton solitons to a standing wave condensate induced by interactions. *Phys. Rev. Lett.*, 120:167402, Apr 2018.
- ¹³Nicolas Pernet, Philippe St-Jean, Dmitry D. Solnyshkov, Guillaume Malpuech, Nicola Carlon Zambon, Quentin Fontaine, Bastian Real, Omar Jamadi, Aristide Lemaître, Martina Morassi, Luc Le Gratiet, Téó Baptiste, Abdelmounaim Harouri, Isabelle Sagnes, Alberto Amo, Sylvain Ravets, and Jacqueline Bloch. Gap solitons in a one-dimensional driven-dissipative topological lattice. *Nature Physics*, 18:678–684, 2022.
- ¹⁴T. Gao, O. A. Egorov, E. Estrecho, K. Winkler, M. Kamp, C. Schneider, S. Höfling, A. G. Truscott, and E. A. Ostrovskaya. Controlled ordering of topological charges in an exciton-polariton chain. *Phys. Rev. Lett.*, 121:225302, Nov 2018.
- ¹⁵Min-Sik Kwon, Byoung Yong Oh, Su-Hyun Gong, Je-Hyung Kim, Hang Kyu Kang, Sooseok Kang, Jin Dong Song, Hyoungsoon Choi, and Yong-Hoon Cho. Direct transfer of light’s orbital angular momentum onto a nonresonantly excited polariton superfluid. *Phys. Rev. Lett.*, 122:045302, Jan 2019.
- ¹⁶Riccardo Panico, Guido Macorini, Lorenzo Dominici, Antonio Gianfrate, Antonio Fieramosca, Milena De Giorgi, Giuseppe Gigli, Daniele Sanvitto, Alessandra S. Lanotte, and Dario Ballarini. Dynamics of a vortex lattice in an expanding polariton quantum fluid. *Phys. Rev. Lett.*, 127:047401, Jul 2021.
- ¹⁷Kirill A. Sitnik, Sergey Alyatkin, Julian D. Töpfer, Ivan Gnusov, Tamsin Cookson, Helgi Sigurdsson, and Pavlos G. Lagoudakis. Spontaneous formation of time-periodic vortex cluster in nonlinear fluids of light. *Phys. Rev. Lett.*, 128:237402, Jun 2022.
- ¹⁸D. Biegańska, M. Pieczarka, E. Estrecho, M. Steger, D. W. Snoke, K. West, L. N. Pfeiffer, M. Syperek, A. G. Truscott, and E. A. Ostrovskaya. Collective excitations of exciton-polariton condensates in a synthetic gauge field. *Phys. Rev. Lett.*, 127:185301, Oct 2021.
- ¹⁹Xinrui Lei, Aiping Yang, Peng Shi, Zhenwei Xie, Luping Du, Anatoly V. Zayats, and Xiacong Yuan. Photonic spin lattices: Symmetry constraints for skyrmion and meron topologies. *Phys. Rev. Lett.*, 127:237403, Dec 2021.
- ²⁰T. Bienaimé, M. Isoard, Q. Fontaine, A. Bramati, A. M. Kamchatnov, Q. Glorieux, and N. Pavloff. Quantitative analysis of shock wave dynamics in a fluid of light. *Phys. Rev. Lett.*, 126:183901, May 2021.
- ²¹A. Amo, T. C. H. Liew, C. Adrados, R. Houdré, E. Giacobino, A. V. Kavokin, and A. Bramati. Exciton-polariton spin switches. *Nature Photonics*, 4:361–366, 2010.
- ²²T. C. H. Liew, I. A. Shelykh, and G. Malpuech. Polaritonic devices. *Physics E*, 43:1543–1568, 2011.
- ²³A. Askitopoulos, A. V. Nalitov, E. S. Sedov, L. Pickup, E. D. Cherotchenko, Z. Hatzopoulos, P. G. Savvidis, A. V. Kavokin, and P. G. Lagoudakis. All-optical quantum fluid spin beam splitter. *Phys. Rev. B*, 97:235303, Jun 2018.
- ²⁴Fei Chen, Hui Li, Hang Zhou, Song Luo, Zheng Sun, Ziyu Ye, Fenghao Sun, Jiawei Wang, Yuanlin Zheng, Xianfeng Chen, Huailiang Xu, Hongxing Xu, Tim Byrnes, Zhanghai Chen, and Jian Wu. Optically controlled femtosecond polariton switch at room temperature. *Phys. Rev. Lett.*, 129:057402, Jul 2022.
- ²⁵Guillermo Munoz-Matutano, Andrew Wood, Mattias Johnsson, Xavier Vidal, Ben Q. Baragiola, Andreas Reinhard, Aristide Lemaître, Jacqueline Bloch, Alberto Amo, Gilles Nogues, Benjamin Besga, Maxime Richard, and Thomas Volz. Emergence of quantum correlations from interacting fibre-cavity polaritons. *Nature Mater.*, 18:213–218, 2019.
- ²⁶Anton V. Zasedatelev, Anton V. Baranikov, Denis Sannikov, Darius Urbonas, Fabio Scafrimuto, Vladislav Yu. Shishkov, Evgeny S. Andrianov, Ullrich Lozovik, Yurii E. and Scherf, Thilo Stoferle, Rainer F. Mahrt, and Pavlos G. Lagoudakis. Single-photon nonlinearity at room temperature. *Nature*, 597:493–497, 2021.
- ²⁷Davide Nigro, Vincenzo D’Ambrosio, Daniele Sanvitto, and Dario Gerace. Integrated quantum polariton interferometry. *Communications Physics*, 3:34, 2022.
- ²⁸A. Verger, C. Ciuti, and I. Carusotto. Polariton quantum blockade in a photonic dot. *Phys. Rev. B*, 73:193306, May 2006.
- ²⁹T. C. H. Liew and V. Savona. Single photons from coupled quantum modes. *Phys. Rev. Lett.*, 104:183601, May 2010.
- ³⁰H. J. Snijders, J. A. Frey, J. Norman, H. Flayac, V. Savona, A. C. Gossard, J. E. Bowers, M. P. van Exter, D. Bouwmeester, and W. Löffler. Observation of the unconventional photon blockade. *Phys. Rev. Lett.*, 121:043601, Jul 2018.
- ³¹Aymeric Delteil, Thomas Fink, Anne Schade, Sven Höfling, Christian Schneider, and Ataç İmamoğlu. Towards polariton blockade of confined exciton-polaritons. *Nature Materials*, 18:219–222, 2019.
- ³²O. Kyriienko, D. N. Krizhanovskii, and I. A. Shelykh. Nonlinear quantum optics with trion polaritons in 2d monolayers: Conventional and unconventional photon blockade. *Phys. Rev. Lett.*, 125:197402, Nov 2020.
- ³³R. Johne, N. A. Gippius, G. Pavlovic, D. D. Solnyshkov, I. A. Shelykh, and G. Malpuech. Entangled photon pairs produced by a quantum dot strongly coupled to a microcavity. *Phys. Rev. Lett.*, 100:240404, Jun 2008.
- ³⁴Álvaro Cuevas, Juan Camilo Lopez Carreno, Blanca Silva, Milena De Giorgi, Daniel G. Suarez-Forero, Carlos Sánchez Munoz, Antonio Fieramosca, Filippo Cardano, Lorenzo Marrucci, Vittorianna Tasco, Giorgio Biasiol, Elena del Valle, Lorenzo Dominici, Dario Ballarini, Giuseppe Gigli, Paolo Mataloni, Fabrice P. Laussy, Fabio Sciarrino, and Daniele Sanvitto. First observation of the quantized exciton-polariton field and effect of interactions on a single polariton. *Science Adv.*, 4:eaa06814, 2018.
- ³⁵Emil V. Denning, Andreas Knorr, Florian Katsch, and Marten Richter. Efficient quadrature squeezing from biexcitonic parametric gain in atomically thin semiconductors. *Phys. Rev. Lett.*, 129:097401, Aug 2022.
- ³⁶Rahul Trivedi, Marina Radulaski, Kevin A. Fischer, Shanhui Fan, and Jelena Vučković. Photon blockade in weakly driven cavity quantum electrodynamics systems with many emitters. *Phys. Rev. Lett.*, 122:243602, Jun 2019.

- ³⁷Jesper Levinsen, Francesca Maria Marchetti, Jonathan Keeling, and Meera M. Parish. Spectroscopic signatures of quantum many-body correlations in polariton microcavities. *Phys. Rev. Lett.*, 123:266401, Dec 2019.
- ³⁸Travis M. Autry, Gaël Nardin, Christopher L. Smallwood, Kevin Silverman, Daniele Bajoni, Aristide Lemaître, Sophie Bouchoule, Jacqueline Bloch, and Steven Cundiff. Excitation ladder of cavity polaritons. *Phys. Rev. Lett.*, 125:067403, Aug 2020.
- ³⁹You Wang, W. Verstraelen, Baile Zhang, Timothy C. H. Liew, and Y. D. Chong. Giant enhancement of unconventional photon blockade in a dimer chain. *Phys. Rev. Lett.*, 127:240402, Dec 2021.
- ⁴⁰Sanjib Ghosh and Timothy C. H. Liew. Quantum computing with exciton-polariton condensates. *npj Quantum Information*, 6:16, 2020.
- ⁴¹Alexey Kavokin, Timothy C. H. Liew, Christian Schneider, Pavlos G. Lagoudakis, Sebastian Klembt, and Sven Höfling. Polariton condensates for classical and quantum computing. *Nat. Rev. Phys.*, 4:435—451, 2022.
- ⁴²Kirill P. Kalinin and Natalia G. Berloff. Simulating ising and n -state planar potts models and external fields with nonequilibrium condensates. *Phys. Rev. Lett.*, 121:235302, Dec 2018.
- ⁴³Holger Suchomel, Sebastian Klembt, Tristan H. Harder, Martin Klaas, Oleg A. Egorov, Karol Winkler, Monika Emmerling, Ronny Thomale, Sven Höfling, and Christian Schneider. Platform for electrically pumped polariton simulators and topological lasers. *Phys. Rev. Lett.*, 121:257402, Dec 2018.
- ⁴⁴Andrzej Opala, Sanjib Ghosh, Timothy C.H. Liew, and Michał Matuszewski. Neuromorphic computing in ginzburg-landau polariton-lattice systems. *Phys. Rev. Applied*, 11:064029, Jun 2019.
- ⁴⁵Thomas Boulier, Maxime J. Jacquet, Anne Maître, Giovanni Lerario, Ferdinand Claude, Simon Pigeon, Quentin Glorieux, Alberto Amo, Jacqueline Bloch, Alberto Bramati, and Elisabeth Giacobino. Microcavity polaritons for quantum simulation. *Advanced Quantum Technologies*, 3(11):2000052, 2020.
- ⁴⁶Giulia Marcucci, Davide Pierangeli, and Claudio Conti. Theory of neuromorphic computing by waves: Machine learning by rogue waves, dispersive shocks, and solitons. *Phys. Rev. Lett.*, 125:093901, Aug 2020.
- ⁴⁷Daniele Bajoni, Pascale Senellart, Esther Wertz, Isabelle Sagnes, Audrey Miard, Aristide Lemaître, and Jacqueline Bloch. Polariton laser using single micropillar GaAs–GaAlAs semiconductor cavities. *Phys. Rev. Lett.*, 100:047401, Jan 2008.
- ⁴⁸Georgios Cstis, Alex Hartsuiker, Edwin van der Pol, Julien Claudon, Willem L. Vos, and Jean-Michel Gérard. Optical characterization and selective addressing of the resonant modes of a micropillar cavity with a white light beam. *Phys. Rev. B*, 82:195330, Nov 2010.
- ⁴⁹Lydie Ferrier, Esther Wertz, Robert Johne, Dmitry D. Solnyshkov, Pascale Senellart, Isabelle Sagnes, Aristide Lemaître, Guillaume Malpuech, and Jacqueline Bloch. Interactions in confined polariton condensates. *Phys. Rev. Lett.*, 106:126401, Mar 2011.
- ⁵⁰B. Real, N. Carlon Zambon, P. St-Jean, I. Sagnes, A. Lemaître, L. Le Gratiet, A. Harouri, S. Ravets, J. Bloch, and A. Amo. Chiral emission induced by optical zeeman effect in polariton micropillars. *Phys. Rev. Research*, 3:043161, Dec 2021.
- ⁵¹E. S. Sedov, V. A. Lukoshkin, V. K. Kalevich, P. G. Savvidis, and A. V. Kavokin. Circular polariton currents with integer and fractional orbital angular momenta. *Phys. Rev. Research*, 3:013072, Jan 2021.
- ⁵²Tintu Kuriakose, Paul M. Walker, Toby Dowling, Oleksandr Kyriienko, Ivan A. Shelykh, Phillipe St-Jean, Nicola Carlon Zambon, Aristide Lemaître, Isabelle Sagnes, Luc Legratiet, Sylvain Harouri, Abdellounaim and Ravets, Maurice S. Skolnick, Alberto Amo, Jacqueline Bloch, and Dmitry N. Krizhanovskii. Few-photon all-optical phase rotation in a quantum-well micropillar cavity. *Nat. Photon.*, 16:566–569, 2022.
- ⁵³Marta Galbiati, Lydie Ferrier, Dmitry D. Solnyshkov, Dimitrii Tanese, Esther Wertz, Alberto Amo, Marco Abbarchi, Pascale Senellart, Isabelle Sagnes, Aristide Lemaître, Elisabeth Galopin, Guillaume Malpuech, and Jacqueline Bloch. Polariton condensation in photonic molecules. *Phys. Rev. Lett.*, 108:126403, Mar 2012.
- ⁵⁴M. Milićević, T. Ozawa, G. Montambaux, I. Carusotto, E. Galopin, A. Lemaître, L. Le Gratiet, I. Sagnes, J. Bloch, and A. Amo. Orbital edge states in a photonic honeycomb lattice. *Phys. Rev. Lett.*, 118:107403, Mar 2017.
- ⁵⁵C. E. Whittaker, E. Cancellieri, P. M. Walker, D. R. Gulevich, H. Schomerus, D. Vaitiekus, B. Royall, D. M. Whittaker, E. Clarke, I. V. Iorsh, I. A. Shelykh, M. S. Skolnick, and D. N. Krizhanovskii. Exciton polaritons in a two-dimensional lieb lattice with spin-orbit coupling. *Phys. Rev. Lett.*, 120:097401, Mar 2018.
- ⁵⁶C. E. Whittaker, T. Dowling, A. V. Nalitov, A. V. Yulin, B. Royall, E. Clarke, M. S. Skolnick, I. A. Shelykh, and D. N. Krizhanovskii. Optical analogue of dresselhaus spin–orbit interaction in photonic graphene. *Nat. Photon.*, 15:193–196, 2021.
- ⁵⁷C. Ciuti, V. Savona, C. Piermarocchi, A. Quattropani, and P. Schwendimann. Role of the exchange of carriers in elastic exciton-exciton scattering in quantum wells. *Phys. Rev. B*, 58:7926–7933, Sep 1998.
- ⁵⁸M. M. Glazov, H. Ouerdane, L. Pillozzi, G. Malpuech, A. V. Kavokin, and A. D’Andrea. Polariton-polariton scattering in microcavities: A microscopic theory. *Phys. Rev. B*, 80:155306, Oct 2009.
- ⁵⁹G. Rochat, C. Ciuti, V. Savona, C. Piermarocchi, A. Quattropani, and P. Schwendimann. Excitonic bloch equations for a two-dimensional system of interacting excitons. *Phys. Rev. B*, 61:13856–13862, May 2000.
- ⁶⁰V. Shahnazaryan, I. A. Shelykh, and O. Kyriienko. Attractive coulomb interaction of two-dimensional rydberg excitons. *Phys. Rev. B*, 93:245302, Jun 2016.
- ⁶¹V. Shahnazaryan, I. Iorsh, I. A. Shelykh, and O. Kyriienko. Exciton-exciton interaction in transition-metal dichalcogenide monolayers. *Phys. Rev. B*, 96:115409, Sep 2017.
- ⁶²E. Snitzer. Cylindrical dielectric waveguide modes*. *J. Opt. Soc. Am.*, 51(5):491–498, May 1961.
- ⁶³Giovanna Panzarini and Lucio Claudio Andreani. Quantum theory of exciton polaritons in cylindrical semiconductor microcavities. *Phys. Rev. B*, 60:16799–16806, Dec 1999.
- ⁶⁴C. Ciuti, V. Savona, C. Piermarocchi, A. Quattropani, and P. Schwendimann. Role of the exchange of carriers in elastic exciton-exciton scattering in quantum wells. *Phys. Rev. B*, 58:7926–7933, Sep 1998.
- ⁶⁵E. L. Ivchenko. *Optical spectroscopy of semiconductor nanostructures*. Alpha Science International Ltd, 2005.
- ⁶⁶Dirk Witthaut, Sandro Wimberger, Raffaella Burioni, and Marc Timme. Classical synchronization indicates persistent entanglement in isolated quantum systems. *Nature Communications*, 8:14829, 2017.
- ⁶⁷José Nuno S. Gomes, Carlos Trallero-Giner, Nuno M. R. Peres, and Mikhail I. Vasilevskiy. Exciton–polaritons of a 2d semiconductor layer in a cylindrical microcavity. *Journal of Applied Physics*, 127(13):133101, 2020.
- ⁶⁸V B Berestetskii, E M Lifshitz, and L P Pitaevskii. *Quantum Electrodynamics*. Butterworth-Heinemann, 2 edition, 1982.